
Proceedings Paper:
Vardhan, H., Odavic, M. orcid.org/0000-0002-2104-8893 and Atallah, K. orcid.org/0000-0002-8008-8457 (2023) Comprehensive analysis and design optimization of the Dual Active Bridge DC-DC converter with finite magnetizing inductance. In: 2023 IEEE Applied Power Electronics Conference and Exposition (APEC). 2023 IEEE Applied Power Electronics Conference and Exposition (APEC), 19-23 Mar 2023, Orlando, FL, USA. Institute of Electrical and Electronics Engineers (IEEE) , pp. 2661-2667. ISBN 9781665475396

https://doi.org/10.1109/apec43580.2023.10131258

Comprehensive analysis and design optimization of the Dual Active Bridge DC-DC converter with finite magnetizing inductance

Harsha Vardhan
Dept. of Electronic and Electrical Eng.
The University of Sheffield
Sheffield, UK
harshavardhan1@sheffield.ac.uk

Milijana Odavic
Dept. of Electronic and Electrical Eng.
The University of Sheffield
Sheffield, UK
m.odavic@sheffield.ac.uk

Kais Atallah
Dept. of Electronic and Electrical Eng.
The University of Sheffield
Sheffield, UK
k.atallah@sheffield.ac.uk

***Abstract*— This research provides an in-depth general analysis of a Dual Active Bridge (DAB) DC-DC converter with a finite magnetizing inductance (L_m). A high-frequency transformer considered in this study is a radial-type rotary transformer for aerospace applications. A single-phase-shift (SPS) modulation technique is considered in this study. First, it develops new analytical equations for the RMS currents of the converter that include the effects of L_m. The analysis is based on the equivalent T-type electric circuit transformer model. Then, this study shows that a high L_m is not the best choice for the overall system performance, including loss and transformer mass, which have a direct effect on the converter's power density. The analysis further shows the effects of different system parameters such as the control phase-shift angle, transformer inductances, turns ratio, and switching frequency on the SPS-DAB performance. Understanding the impact of these parameters on the performance of the DAB can contribute to the optimum design of the converter. The proposed theory and analytical equations are validated by the MATLAB/Simulink simulation of a 40 kW 800V/800V DAB converter switching model.**

Keywords*— *Finite magnetizing inductance, Dual Active Bridge, Rotary transformer, DC-DC converter..

I. INTRODUCTION

In high-voltage and high-power applications where input and output DC voltages are tightly regulated, the Single-Phase-Shift (SPS) modulated Dual Active Bridge (DAB) DC-DC converter is the best option due to its performance and simple control compared to advanced modulation techniques [1–2]. [1] provides a summary of DAB performance based on different modulation schemes; however, magnetizing inductance (L_m) is not included in the analysis. Fig. 1(a) shows the basic DAB converter circuit, while Fig. 1(b) represents the electric circuit with the transformer inductances (L_1, L_2, and L_m) and turns ratio ($q=N_S/N_P$) that characterize the exact transformer. Although several papers [3–8] have discussed the effect of L_m on the performance of the SPS-DAB converter, the value of L_m is selected solely based on the converter's performance to reduce conduction losses and achieve soft-switching operation. The effect of L_m on transformer performance, including mass and temperature, has not been investigated.

[3-5] have used external primary and secondary side inductances (L_1 and L_2) and chosen a high value of L_m compared to L_1 and L_2 to design the transformer, not considering a potential effect on the transformer size. Furthermore, [6–8] have demonstrated an integrated transformer design where the dependences of primary and secondary leakage inductances on L_m are taken into account, but optimal designs considering both transformer mass and loss have not been discussed. Similarly, [9–16] provides a

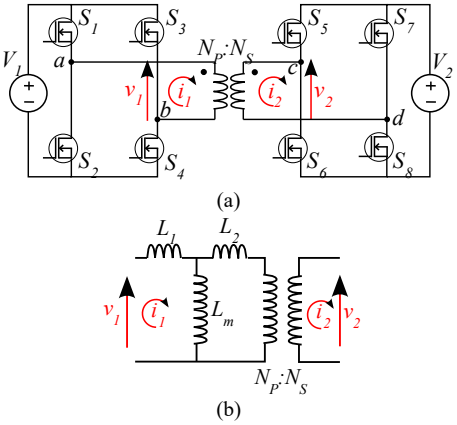

Fig. 1. (a) DAB converter topology, (b) Most common electric circuit representation of the transformer.

comprehensive study of reactive power for optimal design of DAB using various methodologies, while the analytical equations used in this study do not consider L_m. This study thus takes a new approach by considering both transformer and converter performances, demonstrating that selecting L_m solely based on converter performance can result in a not-optimal (oversized) transformer. To design the system (converter and transformer) optimally, analytical equations for RMS currents, including the effect of L_m are needed, and to the best of the authors' knowledge, they are not available in the literature. Furthermore, recent SPS-DAB research [3],[6] reveals some effects of L_m, but analytical equations for active power and peak current assume an infinite L_m. The accurate equations that consider finite L_m for active power and peak current are found in papers [7-8], but they are complex and lack insight. Also, the same complex peak current equations are applied to the Zero Voltage Switching (ZVS) region, making it difficult to represent distinct ZVS regions graphically. As a result, this paper develops new analytical equations for RMS currents, followed by analysis based on the T-type model with simple, intuitive, and exact equations for peak currents, active power, and (ZVS) regions while accounting for L_m.

Furthermore, to demonstrate the effect of L_m on the mass and loss of the system, the optimal transformer design study [16] is further evaluated in this research based on the magnetizing inductance. [16] describes the optimal design methodology for a 40 kW rotary transformer (shown in Fig. 2) based SPS-DAB converter with the specifications listed in Table I. However, the analytical equations for the RMS and peak currents of the transformer, used in [16], ignore the effect of L_m, which influences significantly the converter performance and will be discussed briefly in this study. The objective of the optimization in [16] is to design a radial type rotary

transformer (RT) with minimal total mass and loss, and the optimization algorithm takes care of the transformer's loss and mass and generates the optimal design without explicitly demonstrating the effect of different inductances such as L_1, L_2 and L_m. Thus, in this study, the detailed post-processing of the optimization results based on the exact analytical equation developed in this paper will be presented to demonstrate the effect of transformer inductances on the DAB performance. Understanding the influence of these parameters on the DAB's performance can contribute to the system's optimal design. The proposed theory and analytical equations are validated by simulating a 40 kW 800V/800V DAB converter switching model using RT's electrical model in MATLAB/Simulink.

TABLE I: SPS-DAB CONVERTER SPECIFICATION

Parameter	Symbol	Value
Output Power	P_{out}	40 kW
Input/ Primary side DC Voltage	$V_1 = V_{dc}$	800 V
Output/ Secondary side DC Voltage	$V_2 = V_{dc}$	800 V
Primary and Secondary Duty cycle	$d_P = d_S$	50 %

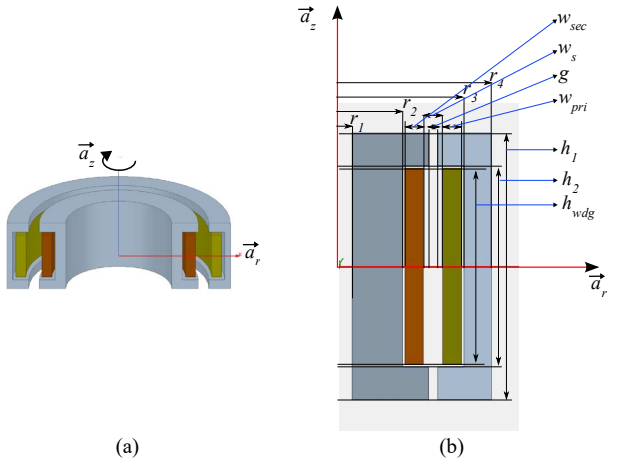

(a) (b)

Fig. 2. (a) Radial type Rotary Transformer and (b) Side view geometry with secondary inner winding and primary outer winding [16].

II. COMPREHENSIVE STEADY-STATE ANALYSIS OF DAB CONVERTER WITH MAGNETIZING INDUCTANCE

The value of magnetizing inductance (L_m) affects the RMS and peak currents, active power, and ZVS region of the DAB converter. So, this section will provide the exact analytical equations and analysis of the DAB converter's performance while taking L_1, L_2 and L_m into account.

A. Equivalent Electrical DAB Model

There are two active full bridges in the DAB converter that are connected via a transformer. Fig. 1(a) is a schematic representation of the DAB converter. The standard equivalent electric circuit of a two-winding conventional transformer is shown in Fig. 3(a), where L_1, L_2, and L_m represent the transformer's primary series inductance, secondary series inductance referred to the primary side, and magnetizing inductance, respectively and q (=N_S/N_P) represents the transformers turns ratio. L_1/L_2 can represent the primary/secondary leakage inductance and any external inductance placed in series on the primary/secondary side of the transformer.

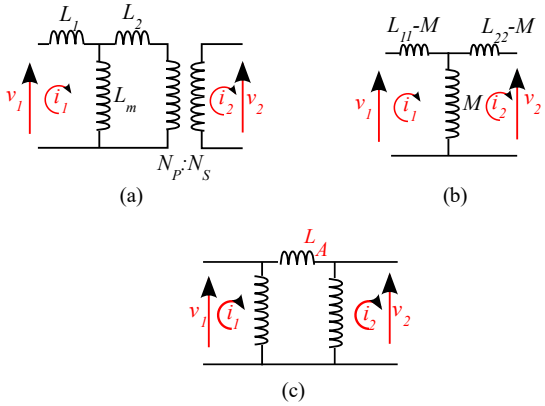

(a) (b) (c)

Fig. 3. (a) Standard equivalent electric circuit, (b) T-type equivalent electric circuit and (c) π-type equivalent electric circuit representation of transformer.

The T-type and π-type electric circuits can be made from the standard electric equivalent circuit, as shown in Figs 3(b) and 3(c), respectively. Assumptions such as comparatively small winding resistances and ideal switches are made to simplify the study of the effect of L_m on performance. Using KVL to determine the Z-parameter matrix (1) on the two-port networks, the inductance matrix can be solved as (2). These inductance matrices can be used to translate the representation of one electric circuit to another (Figs 3(a) and 3(b)), L_{11}, L_{22}, and M are well-known parameters called primary inductance, secondary inductance, and mutual inductance, respectively.

$$\begin{bmatrix} v_1 \\ v_2 \end{bmatrix} = \begin{bmatrix} Z_{11} & Z_{12} \\ Z_{21} & Z_{22} \end{bmatrix} \begin{bmatrix} i_1 \\ -i_2 \end{bmatrix} \tag{1}$$

$$\begin{bmatrix} L_{11} & M \\ M & L_{22} \end{bmatrix} = \begin{bmatrix} L_1 + L_m & qL_m \\ qL_m & q^2(L_2 + L_m) \end{bmatrix} \tag{2}$$

The π-type representation in Fig. 3(c) is useful for determining L_A, the inter-link inductance between the two full bridges that determines the active power flow. L_A can be calculated as (3) by transforming a T-type electric network into a π-type network, where k represents the coupling coefficient. By applying (2) to (3), L_A can also be presented in terms of L_1, L_2 and L_m as (4), which demonstrates the direct effect of various transformer's inductances. With a relatively higher L_m, only the series inductance $q(L_1+L_2)$ incorporates the effective inductance (L_A).

$$L_A = M\left(\frac{1}{k^2} - 1\right);\ k = \frac{M}{\sqrt{L_{11}L_{22}}} \tag{3}$$

$$L_A = q\left(L_1 + L_2 + \frac{L_1 L_2}{L_m}\right) \tag{4}$$

B. RMS and peak current

The current dynamics must first be examined to determine the analytical equation for RMS and peak currents. For the primary and secondary ports of the T-type representation (Fig. 3(b)), the KVL equations can be written as follows:

$$v_1 = L_{11}\frac{di_1}{dt} - M\frac{di_2}{dt} \tag{5}$$

$$v_2 = M\frac{di_1}{dt} - L_{22}\frac{di_2}{dt} \tag{6}$$

By rearranging (5) and (6), the primary and secondary dynamic current equations can be written as, where L_A is given by (3).

$$\frac{di_1}{dt} = \frac{L_{22}}{ML_A}v_1 - \frac{1}{L_A}v_2 \tag{7}$$

$$\frac{di_2}{dt} = \frac{1}{L_A}v_1 - \frac{L_{11}}{ML_A}v_2 \tag{8}$$

These equations determine the shape of the respective current waveforms for any applied modulation technique. In this work, the single-phase-shift (SPS) modulation technique is implemented as shown in Fig. 4. It shows the primary current and pole voltages waveforms with SPS modulation at steady state conditions, for a given switching frequency f_s and $T_s = 1/f_s$, where the secondary voltage v_2 lags the primary voltage v_1 by the phase-shift angle δ.

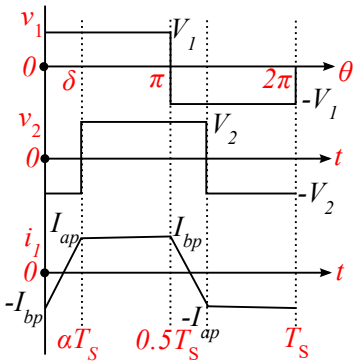

Fig. 4. SPS-DAB pole voltages and primary current waveforms.

Considering half-wave symmetry as shown in the figure, the two slopes of the primary current for 0≤θ≤δ and δ ≤θ≤π can be found by using (7) as follows, where α=δ/2π.

$$\frac{i_1(\delta) - i_1(0)}{\alpha T_s} = \frac{I_{ap} + I_{bp}}{\alpha T_s} = \frac{L_{22}}{ML_A}V_1 - \frac{1}{L_A}(-V_2) = slope_{0,\delta} \tag{9}$$

$$\frac{i_1(\pi) - i_1(\delta)}{(0.5-\alpha)T_s} = \frac{I_{bp} - I_{ap}}{(0.5-\alpha)T_s} = \frac{L_{22}}{ML_A}V_1 - \frac{1}{L_A}(V_2) = slope_{\delta,\pi} \tag{10}$$

By solving these two equations, the peak currents of the primary side I_a and I_b can be found as

$$I_{ap} = i_1(\alpha T_s) = i_1(\delta) = \frac{V_1}{4\pi f_s L_A}\left[2\delta\frac{L_{22}}{M} - \pi\left(\frac{L_{22}}{M} - m\right)\right] \tag{11}$$

$$I_{bp} = i_1(0.5T_s) = i_1(\pi) = -i_1(0) = \frac{V_1}{4\pi f_s L_A}\left[2\delta m + \pi\left(\frac{L_{22}}{M} - m\right)\right] \tag{12}$$

Here, m is the voltage ratio equal to V_2/V_1. Using these equations, the instantaneous primary current $i_1(t)$ can be derived and thus the RMS current on the primary side I_{RMSp} can be calculated as follows:

$$i_1(t) = \begin{cases} (slope_{0,\delta})t + i_1(0) & 0 \le t \le \alpha T_s \\ (slope_{\delta,\pi})(t - \alpha T_s) + i_1(\alpha T_s) & \alpha T_s \le t \le 0.5T_s \end{cases} \tag{13}$$

$$I_{RMSp} = \frac{2}{T_s}\int_0^{0.5T_s} i_1(t)^2\,dt \tag{14}$$

$$I_{RMSp} = \frac{V_1}{2\pi f_s L_A}\sqrt{\frac{1}{12}\left[\pi\left(\frac{L_{22}}{M} - m\right)\right]^2 - \frac{mL_{22}}{3M}\delta^2\left(\frac{2\delta}{\pi} - 3\right)} \tag{15}$$

Similarly, by using (8), peak currents on the secondary side of the transformer at instant θ=δ and θ=π can be calculated as (16) and (17) respectively. The corresponding secondary RMS current I_{RMSs} can be calculated as (18).

$$I_{as} = i_2(\delta) = \frac{V_1}{4\pi f_s L_A}\left[2\delta - \pi\left(1 - m\frac{L_{11}}{M}\right)\right] \tag{16}$$

$$I_{bs} = i_2(\pi) = -i_2(0) = \frac{V_1}{4\pi f_s L_A}\left[2m\delta\frac{L_{11}}{M} + \pi\left(1 - m\frac{L_{11}}{M}\right)\right] \tag{17}$$

$$I_{RMSs} = \frac{V_1}{2\pi f_s L_A}\sqrt{\frac{1}{12}\left[\pi\left(1 - m\frac{L_{11}}{M}\right)\right]^2 - \frac{mL_{11}}{3M}\delta^2\left(\frac{2\delta}{\pi} - 3\right)} \tag{18}$$

In addition, the general analytical equation for the RMS value of the derivative of the currents also can be evaluated as (19) and (20) as it is needed in some applications such as for calculating the effective AC resistance of the litz wire which carries non-sinusoidal current [16].

$$\left\langle\frac{d}{dt}i_1(t)\right\rangle_{RMSp} = \frac{V_1}{L_A}\sqrt{\left(\frac{L_{22}}{M} - m\right)^2 + \frac{4\delta mL_{22}}{\pi M}} \tag{19}$$

$$\left\langle\frac{d}{dt}i_2(t)\right\rangle_{RMSs} = \frac{V_1}{L_A}\sqrt{\left(1 - m\frac{L_{11}}{M}\right)^2 + \frac{4\delta mL_{11}}{\pi M}} \tag{20}$$

C. Active Power

The power transfer characteristics of the SPS-DAB converter can now be calculated by averaging the product of instantaneous primary current i_1 (13) and pole voltage v_1. Thus, the total active power transferred can be derived as (22), and it can be seen that the expression is similar to that of the ideal-SPS-DAB converter [1]; this can be explained using the π-type electric circuit representation, in which two voltage sources transfer power through inter-link inductance L_A (4). The maximum power transfer can be calculated at δ= π /2 as (23).

$$P_{out} = \frac{1}{0.5T_s}\int_0^{0.5T_s} i_1(t)v_1(t)dt \tag{21}$$

$$P_{out} = \frac{V_1V_2}{2\pi f_s L_A}\left(\delta\left(1 - \frac{|\delta|}{\pi}\right)\right);\ \text{for}\ -\pi \le \delta \le \pi \tag{22}$$

$$P_{out_{max}} = \frac{mV_1{}^2}{2\pi f_s L_A}\frac{\pi}{4};\ at\ \delta = \frac{\pi}{2}\ \ where, m = \frac{V_2}{V_1} \tag{23}$$

From (22) and (4), it can be concluded that the power transfer capability reduces with the finite L_m. Furthermore, from (22), the solution of the phase-shift angle δ for the given output power can be found as (24).

$$\delta = \frac{\pi}{2}\left[1 - \sqrt{1 - \left(\frac{8f_sL_AP_{out}}{V_1V_2}\right)}\right] \tag{24}$$

D. ZVS Region

Both primary and secondary switches of the SPS-DAB converter can be turned on and off at zero voltage switching (ZVS) instants [2]. From no load to full load, there are regions

in the operating area where ZVS happens under certain conditions. The conditions for assuring ZVS for secondary switches (i.e., at switching instant θ=δ) and for primary switches (i.e., at switching instant θ=π) are given by (24) and (25). These conditions also assure ZVS for the switching instants in the second half of the period because of the half-way symmetry, i.e., at θ=(π+δ) (secondary switches) and θ=0 (primary switches).

$$i_2(\delta) > 0 \ : \text{ZVS for secondary switches} \tag{25}$$

$$i(\pi) > 0 \ : \text{ZVS for primary switches} \tag{26}$$

Thus, using (16) and (12) together with (25) and (26), the ZVS condition considering the effect of Lm can be found as follows:

$$\delta > \frac{\pi}{2}\left(1 - m\frac{L_{11}}{M}\right) \tag{27}$$

$$\delta > \frac{\pi}{2}\left(1 - \frac{L_{22}}{mM}\right) \tag{28}$$

The presented comprehensive analysis is proposed for improved design and analysis of a DAB converter and an associated transformer with finite Lm. These analytical equations are used in the following section to analyze the impact of Lm on the mass and loss of the RT, which directly impact the power density of the converter.

III. Data Post-Processing and Evaluation of a Rotary Transformer with Magnetizing Inductance

This section demonstrates the impact of L_m on the transformer's mass and loss by post-processing the data of all RT design candidates based on Table I and [16]. The magnetic, electrical, and thermal properties of RT are modelled in detail in [16], and the same optimal design algorithm and inputs are used for further analysis in this paper.

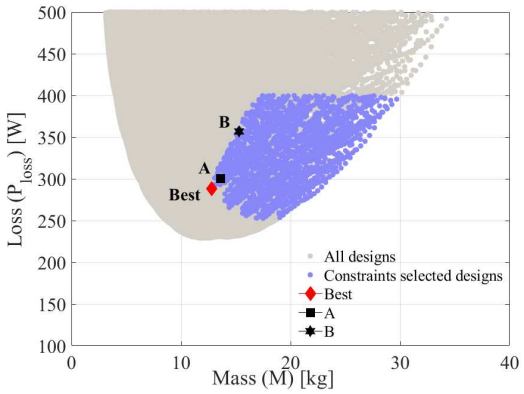

Fig. 5. Loss vs. mass trends of all possible and constraints filtered RT designs for specifications listed in Table I and [16].

According to the research in [16], the six input optimisation variables (OVs): operating flux density, number of primary & secondary turns, switching frequency and number of strands and diameter of each strand in the Litz wire are required for the construction of RT, and running the optimization engine for multiple iterations can provide the optimal design, as shown in Fig. 5. Detailed information about Fig. 5 is available in [16], which depicts all valid RT design candidates in terms of total loss and mass for the specifications listed in Table I. In addition, the research reveals complex design trends involving different system parameters, such as operating frequency (10 kHz to 100 kHz), number of turns, and core thickness.

In this paper, the same analysis is performed to gain a deeper understanding of the influence of the transformer's inductances and optimization results based on the exact analytical equations developed in this paper. In Table II, the design results of the optimization process for three cases have been listed. The first case (*Best*) demonstrates the optimal design and parameters that stay true to all practical constraints and have the minimum mass solution. In contrast, the second (*A*) and third (*B*) cases were chosen rationally to demonstrate the impact of L_m. All of the symbols used to describe the parameters and geometry of RT listed in Table II are depicted in Figs. 1(b) and 2(b). These design cases are also marked in Fig. 5. In this study, constraints like core thickness > 10 mm, phase-shift angle > 30º, and max. temperature < 180 ºC are used. The geometrical parameters for the RT designs for different cases are listed in Table II. By selecting the cases with the same number of turns of litz wire, the winding area is kept identical to understand the effect of geometry on various inductances.

TABLE II: Optimal Chosen Designs And Their Respective Parameters For 40 KW 800V/800V RT-Based DAB Converter

Parameters	Symbol	Best	A	B	Units
Operating Flux density	B	64.3	61.4	56.2	mT
No. of Primary/ Secondary Turns	$N_P = N_S$	4	4	4	–
Switching Frequency	f_s	45	45	45	kHz
No. of Strands in Litz wire	N_{str}	2000	2000	2000	–
Diameter of each strand in Litz wire	d_{str}	0.07	0.07	0.07	mm
Total Loss	P_{loss}	**288.3**	**300.5**	**356.8**	W
Core Loss	P_{iGSE}	47.6	45.2	41.5	W
Winding Loss	$P_{wdg.loss}$	240.7	255.3	315.3	W
Total Mass	M	**12.8**	**13.6**	**15.3**	kg
Max. Temperature	T_{MAX}	176	176	179	ºC
Core thickness	$r_2 - r_1$	10	10.5	11.4	mm
DAB phase-shift angle	δ	31	35.9	53.6	º
Output Power	P_{out}	40	40	40	kW
Pri Current RMS	I_{RMSp}	58.6	60.1	66.1	A
Magnetising inductance ref. to pri. Side	L_m	**225**	**234**	**254**	µH
Pri. series inductance	L_1	12.5	13.9	18.1	µH
Sec. series inductance ref. to pri. Side	L_2	12.2	13.7	17.8	µH
Inter-link inductance	L_A	25.3	28.4	37.2	µH
Shaft Radius	r_1	270	270	270	mm
Inner radius 1	r_2	280	280.5	281.4	mm
Inner radius 2	r_3	301.5	303.1	307.3	mm
Outer Radius	r_4	310.5	312.5	317.4	mm
Air gap length	g	1	1	1	mm
Gap length b/w windings	w_s	5	5	5	mm
Pri. / Sec. winding width	$w_{pri} = w_{sec}$	7.2	7.8	9.4	mm
Outer core height	h_1	35	35	35	mm
Inner core height	h_2	12.6	11.7	9.7	mm

Fig. 6 shows the different RT designs for the three cases listed in Table II. Table II or Fig. 6 shows that the magnetizing inductance is directly proportional to the core thickness, while the leakage inductance is directly proportional to the aspect ratio of the winding window's width and height for the same number of turns. Detailed analytical equations for these

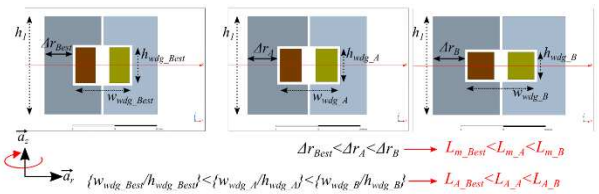

Fig. 6. Comparing the geometry of RT design for different cases: Best. A and B (left to right).

inductances for radial type RT are provided in [16]. Furthermore, from Table II, it can also be seen that even though case B has a larger magnetizing inductance than case A, case B has a higher winding loss and, consequently, a higher total loss for the same 40 kW and 800/800 V DAB operation. Further, this trend can be seen widely for all the RT designs, as shown in Figs. 7(a) and 7(b) for the loss and mass versus L_m. This demonstrates that selecting a higher L_m leads to an increase in both loss and mass.

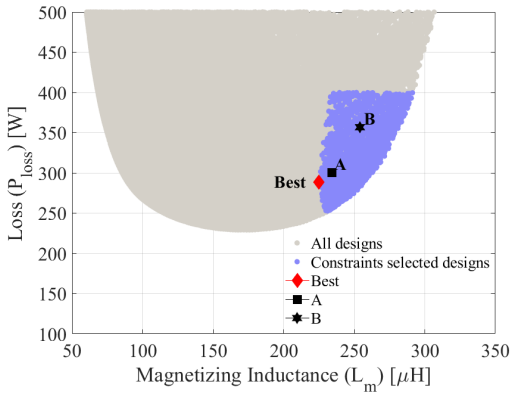

(a) Loss vs Magnetizing Inductance

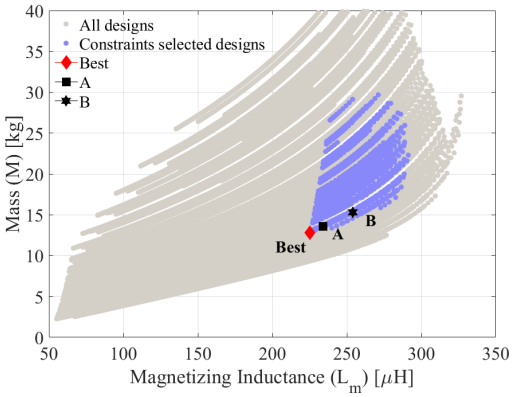

(b) Mass vs Magnetizing Inductance

Fig. 7. All possible and constraints filtered RT designs for specifications (listed in Table I and [16])

It is unusual for an increase in L_m value to increase conduction loss or RMS currents. In this RT case, this is because of the interdependence between L_m and inter-link inductance (L_A), where L_A is significantly determined by the leakage inductances, as can be seen in (4). The relationship between L_m and L_A, on the other hand, is primarily based on geometry and can vary depending on the method used to design the transformer geometry. The relationship is revealed in this study through simple post-processing of the RT designs, as shown in Fig. 8(a), and it can be seen that L_A increases in proportion to L_m. This figure includes only the designs that fulfill the above mentioned system constraints for meaningful results. Furthermore, because L_A is the inter-link inductance between the two full bridges that control the RMS currents for a specific output power, as shown in Fig. 8(b), L_A significantly increases the RMS current (at various frequencies) and consequently the losses. Consequently, in this design case, with an increase in L_m, both the loss and mass are increasing and affecting the overall system performance.

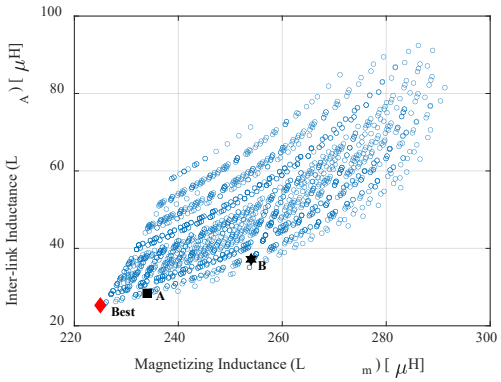

(a) Inter-Link Inductance vs Magnetizing Inductance

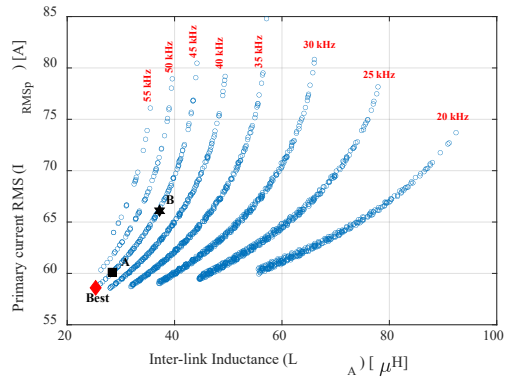

(b) Primary RMS current vs Inter-Link Inductance

Fig. 8. Only constraints filtered RT designs for specifications (listed in Table I and [16])

For the DAB specification listed in Table I, Fig. 9 shows the design trends for the inter-link inductance L_A considering switching frequency and phase-shift angle δ. An optimal design can then be chosen using Figs. 8(b) and 9. Lowering the phase shift angle for a given power load at a particular frequency to reduce the required L_A can thus increase power density.

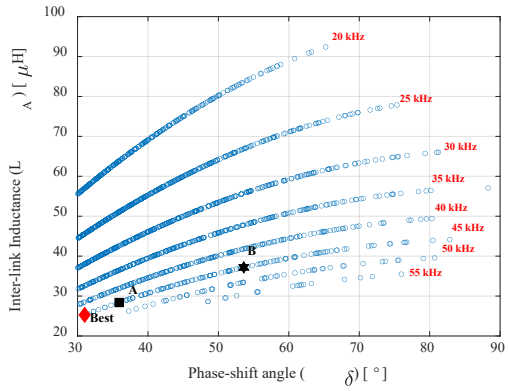

Fig. 9. Inter-link inductance required vs phase shift angle with different frequencies for control of a DAB converter for specifications (listed in Table I and [16]).

A. *Discussion and validation of the analytical models*

[16] uses the approximate analytical equations for the peak and RMS currents as given by (29) and (30) for V_1=V_2=800V and N_P:N_S=1:1 configuration. Because of the unity turns ratio, it assumes the same current flowing in both primary and secondary windings as given below. The proposed exact equations (11)-(18) also simplify to (29),(30) by setting L_m = infinite.

$$I_{ap} = I_{bp} = I_{as} = I_{bs} = \frac{\delta V_1}{2\pi f_s L_A} \tag{29}$$

$$I_{RMSp} = I_{RMSs} = \frac{\delta V_1}{2\pi f_s L_A}\sqrt{1-\frac{2\delta}{3\pi}} \tag{30}$$

However, using the exact analytical model presented in this paper (11–18), the accuracy of the optimization results can be evaluated. For this firstly, the analytical equation developed in this paper has been validated using the *Best* case (Table II) as shown in Table III.

TABLE III: TRANSFORMER PARAMETERS FOR MATLAB SIMULATION

Parameters	Symbol	Best	Units
No. of Primary/ Secondary Turns	$N_P = N_S$	4	_
Switching Frequency	f_s	45	kHz
Magnetising inductance ref. to pri. Side	L_m	225	µH
Pri. series inductance	L_1	12.5	µH
Sec. series inductance ref. to pri. Side	L_2	12.2	µH
Inter-link inductance	L_A	25.3	µH

Fig. 10 shows the validation of the proposed analytical equation for current stress considering with and without L_m vs MATLAB simulation and it can also be seen that the impact of L_m on the no-load RMS current is more as compared to the full-load RMS current.

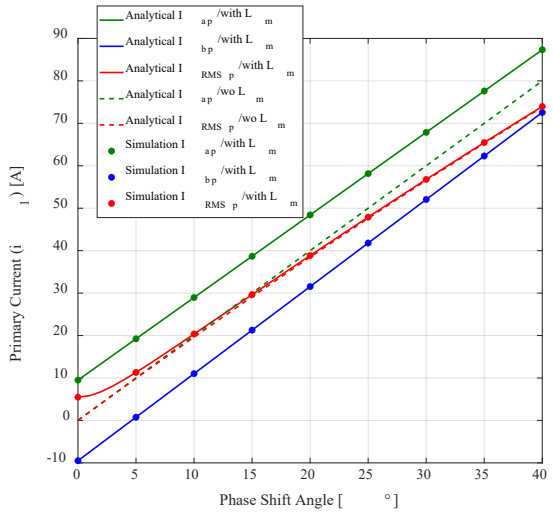

Fig. 10. Validation of the proposed analytical equation for current stress with and without L_m for 800/800 V and other specifications are listed in Table III.

Table IV compares the exact and approximate analytical equation results of the current RMS and peak values for full-load and light-load conditions. It can be seen that the RMS current has < 5% error at full load, and hence the optimization results presented in [16] are valid. However, at light-load conditions, the accuracy of the model is impacted by L_m (as shown in Table IV), and thus the exact equation needs to be used for the optimization purpose.

TABLE IV: COMPARISON OF CURRENT STRESS WITH EXACT AND APPROXIMATE ANALYTICAL [16] EQUATIONS

Parameters	Exact	[16]	% Error
Full Load (40 kW)			
Output Power (P_{out}) (kW)	40	40	_
DAB phase-shift (δ)angle (º)	31	31	_
Pri Current RMS (I_{RMSp}) (A)	58.62	56.84	-3.1%
Sec Current RMS (I_{RMSs}) (A)	58.67	56.84	-3.2%
Pri Peak current (I_{ap}) (A)	69.92	60.43	-15.7%
Pri Valley current (I_{ap}) (A)	54.20	60.43	10.3%
Sec Peak current (I_{as}) (A)	54.05	60.43	10.6%
Sec Valley current (I_{bs}) (A)	70.15	60.43	-16.1%
Light Load (10 % of Full load)			
Output Power (P_{out}) (kW)	4	4	_
DAB phase-shift (δ)angle (º)	2.6	2.6	_
Pri Current RMS (I_{RMSp}) (A)	7.55	5.05	-49.4%
Sec Current RMS (I_{RMSs}) (A)	7.65	5.05	-51.4%
Pri Peak current (I_{ap}) (A)	14.57	5.07	-187.2%
Pri Valley current (I_{ap}) (A)	-4.15	5.07	181.7%
Sec Peak current (I_{as}) (A)	-4.37	5.07	186.2%
Sec Valley current (I_{bs}) (A)	14.80	5.07	-191.8%

Furthermore, although the RMS current error is small at full load conditions (Table IV), the peak currents, which determine the selection of the converter's switches, are significantly higher when L_m is considered. Thus, the SPS-DAB converter performance can be well optimized when considering L_m by using the exact solution. Additionally, the impact of L_m can be seen in the soft-switching operation as well. As expected, it is found that with finite L_m the ZVS region expands. Also, it is evident that by selecting a voltage ratio equal to the turn ratio, the ZVS can be obtained in the full operating area from no load to full load. At other voltage ratio levels, the minimum power limit for ZVS is indicated on the graph, which is governed by (27) and (28) for secondary and primary side switches, respectively. Fig. 11 shows the ZVS regions for different power and output voltage levels for specifications listed in Table III at V_1=800V.

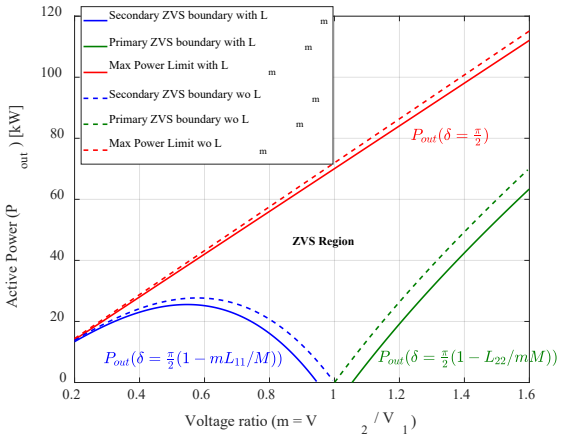

Fig. 11. ZVS region with and without Lm; Impact of Lm on DAB converter ZVS regions for 800V input and other specifications are listed in Table III.

IV. CONCLUSION

This research investigates the optimal design of the SPS-DAB system by considering both transformer and converter performance, demonstrating that selecting L_m solely based on converter performance can result in a non-optimal (oversized) transformer. For designing the system (converter and transformer) optimally, exact analytical equations for peak and RMS currents, including L_m are also provided and compared with the approximate solutions. This analysis takes into account the various impacts of transformer inductances, turns ratio, phase-shift angle, and switching frequency on the performance of the converter, including soft switching region conditions. This research introduces generic and simple equations that significantly govern the DAB's performance. Thus, following this research, the design of the DAB can be improved by having a better understanding of the impact that various system parameters have on the performance of the DAB.

REFERENCES

[1] N. Noroozi, A. Emadi and M. Narimani, ‘‘Performance Evaluation of Modulation Techniques in Single-Phase Dual Active Bridge Converters,’’ in *IEEE Open Journal of the Industrial Electronics Society*, vol. 2, pp. 410-427, 2021.

[2] D. Das and K. Basu, ‘‘Optimal Design of a Dual-Active-Bridge DC–DC Converter,’’ in *IEEE Transactions on Industrial Electronics*, vol. 68, no. 12, pp. 12034-12045, Dec. 2021.

[3] X. Chen, G. Xu, H. Han, D. Liu, Y. Sun and M. Su, ‘‘Light-Load Efficiency Enhancement of High-Frequency Dual-Active-Bridge Converter Under SPS Control,’’ in *IEEE Transactions on Industrial Electronics*, vol. 68, no. 12, pp. 12941-12946, Dec. 2021.

[4] Y. Cai, C. Gu, J. Yang, J. Li, G. Buticchi and H. Zhang, ‘‘An Advanced Extended Phase Shift Modulation Strategy of Daul Active Bridge Converter Considering Magnetizing Inductance,’’ *IECON 2021 – 47th Annual Conference of the IEEE Industrial Electronics Society*, 2021, pp. 1-6.

[5] S. Anwar and D. Costinett, ‘‘Modeling Dual Active Bridge Converter Considering the Effect of Magnetizing Inductance for Electric Vehicle Application,’’ *2018 IEEE Energy Conversion Congress and Exposition (ECCE)*, 2018, pp. 538-545.

[6] E. S. Lee, J. H. Park, M. Y. Kim and S. H. Han, ‘‘An Integrated Transformer Design With a Center-Core Air-Gap for DAB Converters,’’ in *IEEE Access*, vol. 9, pp. 121263-121278, 2021.

[7] S. Anwar and D. Costinett, ‘‘Modeling Dual Active Bridge Converter Considering the Effect of Magnetizing Inductance for Electric Vehicle Application,’’ *2018 IEEE Energy Conversion Congress and Exposition (ECCE)*, 2018, pp. 538-545.

[8] J. Riedel, D. G. Holmes, B. P. McGrath and C. Teixeira, ‘‘Maintaining Continuous ZVS Operation of a Dual Active Bridge by Reduced Coupling Transformers,’’ in *IEEE Transactions on Industrial Electronics*, vol. 65, no. 12, pp. 9438-9448, Dec. 2018.

[9] Y. Xiao, Z. Zhang, M. A. E. Andersen and K. Sun, ‘‘Impact on ZVS Operation by Splitting Inductance to Both Sides of Transformer for 1-MHz GaN Based DAB Converter,’’ in *IEEE Transactions on Power Electronics*, vol. 35, no. 11, pp. 11988-12002, Nov. 2020.

[10] H. Bai and C. Mi, ‘‘Eliminate Reactive Power and Increase System Efficiency of Isolated Bidirectional Dual-Active-Bridge DC–DC Converters Using Novel Dual-Phase-Shift Control,’’ in *IEEE Transactions on Power Electronics*, vol. 23, no. 6, pp. 2905-2914, Nov. 2008.

[11] S. Wang, Z. Zheng, C. Li, K. Wang and Y. Li, ‘‘Time Domain Analysis of Reactive Components and Optimal Modulation for Isolated Dual Active Bridge DC/DC Converters," in *IEEE Transactions on Power Electronics*, vol. 34, no. 8, pp. 7143-7146, Aug. 2019.

[12] H. Shi et al., ‘‘Minimum-Backflow-Power Scheme of DAB-Based Solid-State Transformer With Extended-Phase-Shift Control,’’ in *IEEE Transactions on Industry Applications*, vol. 54, no. 4, pp. 3483-3496, July-Aug. 2018.

[13] H. Wen, W. Xiao and B. Su, ‘‘Nonactive Power Loss Minimization in a Bidirectional Isolated DC–DC Converter for Distributed Power Systems,’’ in *IEEE Transactions on Industrial Electronics*, vol. 61, no. 12, pp. 6822-6831, Dec. 2014.

[14] M. Mu, L. Xue, D. Boroyevich, B. Hughes and P. Mattavelli, "Design of integrated transformer and inductor for high frequency dual active bridge GaN Charger for PHEV," *2015 IEEE Applied Power Electronics Conference and Exposition (APEC),* 2015, pp. 579-585.

[15] Bin Li, Qiang Li, Fred C. Lee, "High-Frequency PCB Winding Transformer With Integrated Inductors for a Bi-Directional Resonant Converter", *IEEE Transactions on Power Electronics,* vol.34, no.7, pp.6123-6135, 2019.

[16] H. Vardhan, M. Odavic and K. Atallah, "Design Optimization Methodology for High-Frequency Rotary Transformers for Contactless Power Transfer Systems," *2022 IEEE Energy Conversion Congress and Exposition (ECCE)*, 2022.

ACKNOWLEDGMENT

This work is funded through the Clean Sky 2 Joint Undertaking (JU); i.e., the project JTI-CS2-2019-CfP10-LPA-01-77.

DISCLAIMER

This work reflects only the authors' views, and the JU is not responsible for any use that may be made of the information it contains.